Available online at www.sciencedirect.com
ScienceDirect
C. R. Physique 9 (2008) 729–740
COMPTES RENDUS PHYSIQUE
http://france.elsevier.com/direct/COMREN/

The dynamo effect/L'effet dynamo

# The Karlsruhe two-scale dynamo experiment

Ulrich Müller [a,*], Robert Stieglitz [a], Fritz H. Busse [b], Andreas Tilgner [c]

[a] *Institute of Nuclear and Energy Technologies, Forschungszentrum Karlsruhe (FZK), P.B. 3640, 76021 Karlsruhe, Germany*
[b] *Institute of Physics, University of Bayreuth, 95440 Bayreuth, Germany*
[c] *Institute of Geophysics, University of Göttingen, 37075 Göttingen, Germany*

Available online 30 August 2008

**Abstract**

This article outlines the experimental realization of the Roberts–Busse kinematic dynamo model at the Forschungszentrum Karlsruhe. Essential observations of the spatial and temporal structures of the self-induced magnetic field and features of its saturation mechanism are presented and the experimental findings are compared with predictions from model calculations. ***To cite this article: U. Müller et al., C. R. Physique 9 (2008).***


**Résumé**

**Le modèle de dynamo cinématique au Forschungszentrum Karlsruhe.** L'article ci-dessous souligne les traits essentiels de la réalisation expérimentale du modèle de dynamo cinématique de Roberts et Busse, au Forschungszentrum Karlsruhe. Nous y présentons les caractéristiques essentielles concernant les structures spatiales et temporelles du champ auto-entretenu. Nous comparons les observations expérimentales avec les prédictions de modèles et de simulations numérique. ***Pour citer cet article : U. Müller et al., C. R. Physique 9 (2008).***


*Keywords:* Dynamo; Magneto-hydrodynamics; Helical channel flow

*Mots-clés :* Dynamo ; Magnéto-hydrodynamique

## 1. Introduction

Today it is generally recognized that planetary and stellar magnetic fields originate from dynamo action in the interior of celestial bodies sustained by buoyancy driven swirling flows in their highly conducting fluid cores. Larmor [1] first hypothesized this idea for the Sun's magnetic field but, naturally, it applies to other celestial objects such as the Earth with its magnetic dipole field as well. Two fundamental questions arise immediately from his hypothesis. Which kind of velocity fields can give rise to dynamo action? What kind of flow structures develop in the liquid cores of rotating planets and stars by the internally acting buoyancy forces and how do they induce magnetic fields which may react back on the flow field? Both questions have been extensively investigated as reflected in recent reviews by P.H. Roberts [2], Roberts and Glatzmaier [3], Busse [4], Glatzmaier [5]. At the beginning, the kinematic dynamo

* Corresponding author.
*E-mail address:* ulrich.rom.mueller@web.de (U. Müller).

1631-0705/$ – see front matter 
doi:10.1016/j.crhy.2008.07.005

problem was in the focus. Various velocity fields with different symmetry properties and dimensional scales have been identified as a potential source for generating large scale magnetic fields. In some pioneering experiments on centrifugally driven convection in rapidly rotating spherical shells Carrigan and Busse [6,7] observed, as a typical feature, arrays of columnar vortices with axes parallel to the axis of rotation which formed at the equatorial rim of the inner shell boundary according to the Taylor Proudman theorem. These observations have drawn particular attention to small scale three-dimensional vortex fields such as those considered by Gailitis [8] and later by G.O. Roberts [9] with periodic properties in one plane and homogeneous or quasi homogeneous behavior perpendicular to this plane, simulating in some kind internal stellar vortex systems.

Based on his observations Busse [10,11] developed a simplified, nevertheless, consistent magneto-hydrodynamic model for the geodynamo featuring the main properties of the geomagnetic field: the dipolar character, its long term steadiness and the close alignment of the dipole with the axis of rotation. Regarding the essential aspects, Busse's analytical geodynamo model and the early experimental findings have been corroborated and extended by several other research groups employing elaborate numerical methods and sophisticated measuring techniques to analyse the vortical structures in rapidly rotating spherical shells filled with liquids of moderate and very low Prandtl numbers such as water and liquid metals (Christensen et al. [12], Aubert et al. [13]). To close the gap between theoretical understanding and experimental observation of dynamo action Busse [14,15] proposed a dynamo-demonstration experiment in the laboratory. The conceptual idea of his proposal was to enclose a large but finite quantity of Roberts's [9] infinitely extended periodic vortex assembly in a finite cylindrical volume (see Fig. 1(a)) and enforce the flow in the individual sections by external pumping power. Using the separation of scales between velocity and magnetic field, an approximate solution for this type kinematic dynamo can be derived in terms of a condition for its onset and an estimate for the dimensions of a feasible experiment. Defining magnetic Reynolds numbers $Re_{mH} = u_H a/\lambda$, $Re_{mC} = u_C a/\lambda$ with the mean helical and axial velocities $u_H$, $u_C$, the diameter $a$ of a vortex, and the magnetic diffusivity $\lambda$ a relationship of the kind $Re_{mC} Re_{mH} > 4\pi^2 \frac{a}{H}[1 + 1.149(H/R)^2]$ is obtained with $H$ the height and $R$ the radius of the bounding cylinder. This simple relation suggested that velocities of the order of 1 m/s had to be achieved in an experimental test volume of $V = 2\pi RH \cong 1 - 4\ \mathrm{m}^3$ liquid sodium. For the final technical design Tilgner [16,18] and Rädler et al. [20,22] developed more accurate approaches to predict conditions for the onset of dynamo action and to characterize topological properties of the generated magnetic field. The results from these calculations will be discussed in Section 4 and be compared with experimental findings. Based on Busse's conceptual proposal the Karlsruhe dynamo test facility was designed and the experimental program was conducted.

## 2. The design of the test facility

The dynamo test module was designed under the premise that for an available pumping capacity a sufficient flow rate for self-excitation of a magnetic field could be achieved. This required a fluid dynamic optimization of the vortex generating channel system with regard to pressure losses. The rectangular vortex containing channels of the G.O. Roberts flow were replaced by vortex generators constructed as coaxial annular channels with helical baffles in the annulus to generate the helical flow and a central pipe through which the central flow could be varied independently. The helical and the axial channels were interlinked at their ends by junctions. A semi-technical sketch of the module is shown in Fig. 1.

In pretests a pressure drop correlation for the flow in the helical ducts was derived containing the following parameters: $Z$ the number of vortex generators, $\chi$ the number of windings per vortex generator, $a$ the diameter of the outer tube, $\Delta r$ the distance between inner and outer tube, $h$ the height of each winding and $\rho$ the density of the liquid sodium and $R/H$ an effective aspect ratio. The optimization resulted in critical magnetic Reynolds numbers $Re_m$ of less than 10 or in technical terms of volumetric flow rates required for self-excitation of $\dot{V}_C = \dot{V}_H = 115 - 143\ \mathrm{m}^3/h$ with the following parameters: $Z = 52$, $a = 0.21$ m, $h = 0.19$ m, $\Delta r = 0.055$ m, $R/H = 1.21$, $\chi = 3.7$. The module was fabricated entirely of stainless steel. Taking into account the different specific conductivities of steel and sodium at the operational temperatures between $120\,^\circ\mathrm{C} < T < 125\,^\circ\mathrm{C}$ a mean magnetic diffusivity of $\lambda \cong 0.1\ \mathrm{m}^2/\mathrm{s}$ was evaluated for the test module. The sodium flow for the system was provided by three independent loops each equipped with an MHD-pump of a feed capacity of up to $\dot{V} \leqslant 150\ \mathrm{m}^3/h$. Two loops supplied the helical and a third one the axial flow channels. The sodium volumetric flow rate provided by MHD pumps was measured by electromagnetic flow meters in each loop. The pressure drop in each of the three independent flow channel-systems was recorded by sensitive capacitance pressure gauges. The module was placed in a room in which the average environmental magnetic

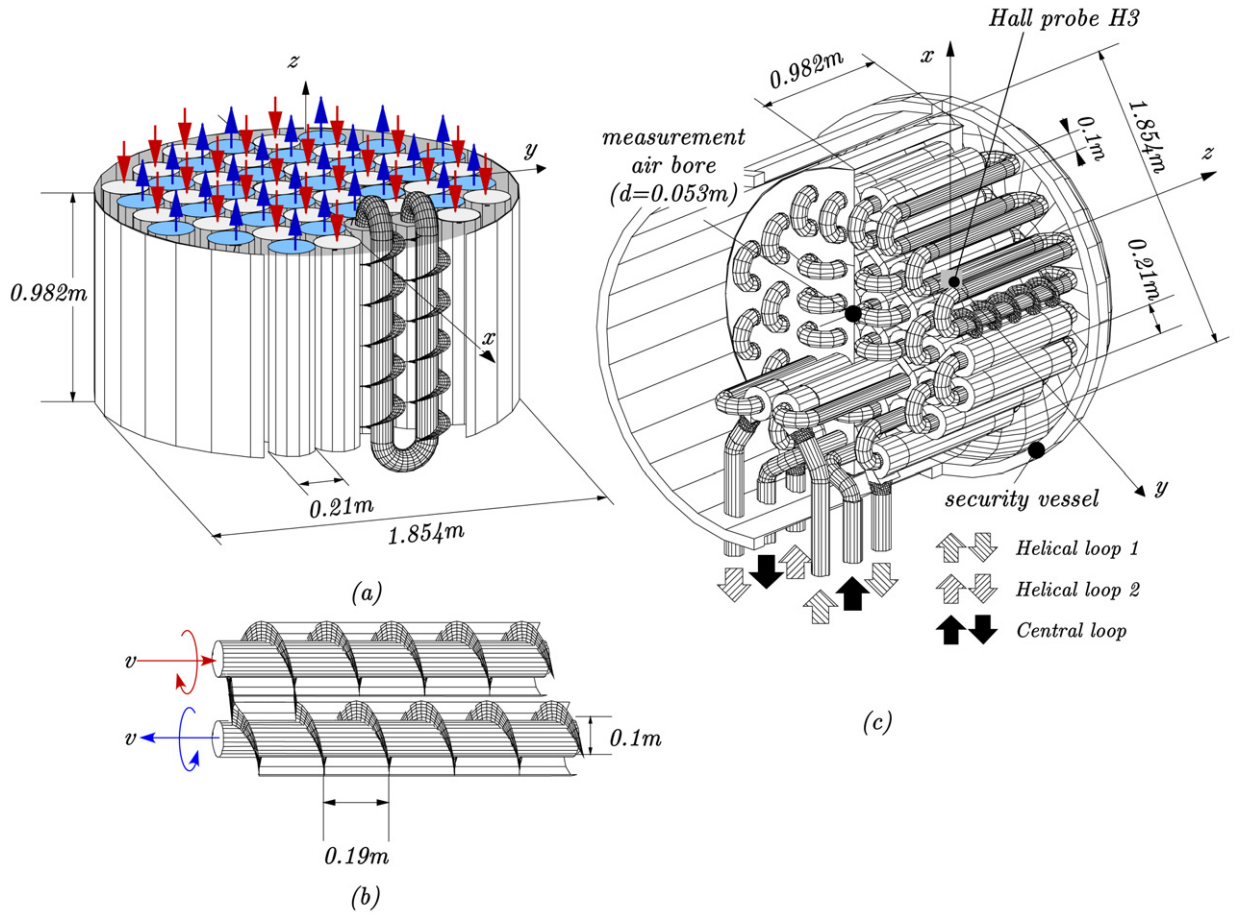


Fig. 1. Sketch of the Karlsruhe dynamo test module: (a) internal structure and principle velocity distribution; (b) vortex generator; (c) technical design with reference coordinate system.

field strength was less than 0.5 Gauss. The dynamo's magnetic field was measured by six Hall-probes and, moreover, sensed by six global induction coils. The location of the most relevant local Hall probe is indicated in Fig. 1(b). During the dynamo tests the magnetic field components were recorded at two fixed locations near the equator of cylinder, and on variable positions in a bore-hole along the cylinder axis between the center and the lid using a traversable probe. The local sodium velocity was measured in the center of one of the four axial channels located next to the axis of the module. This was done with the help of a permanent magnet potential probe (PMP) whose technical details have been described in Müller et al. [23]. A more detailed description of the overall experimental set-up, the sodium technologies and first results may be taken from reports by Stieglitz and Müller [25–27].

## 3. Results

The results reported next will address the following key aspects of the Roberts–Busse kinematic-Dynamo: (a) the onset of dynamo action dependent on particular flow rates; (b) the structure of the observed magnetic field at near- and super-critical flow conditions; (c) the back-reaction of the magnetic field on pressure losses due to Joule dissipation and on the local velocity due to Hartmann effects; and (d) some properties of the small scale temporal fluctuations of the magnetic field.

### *3.1. Onset of dynamo action*

An exemplary demonstration for the initiation and development of the magnetic field is given in Fig. 2 which displays time series of the local components of the generated magnetic field, measured in the center of the module

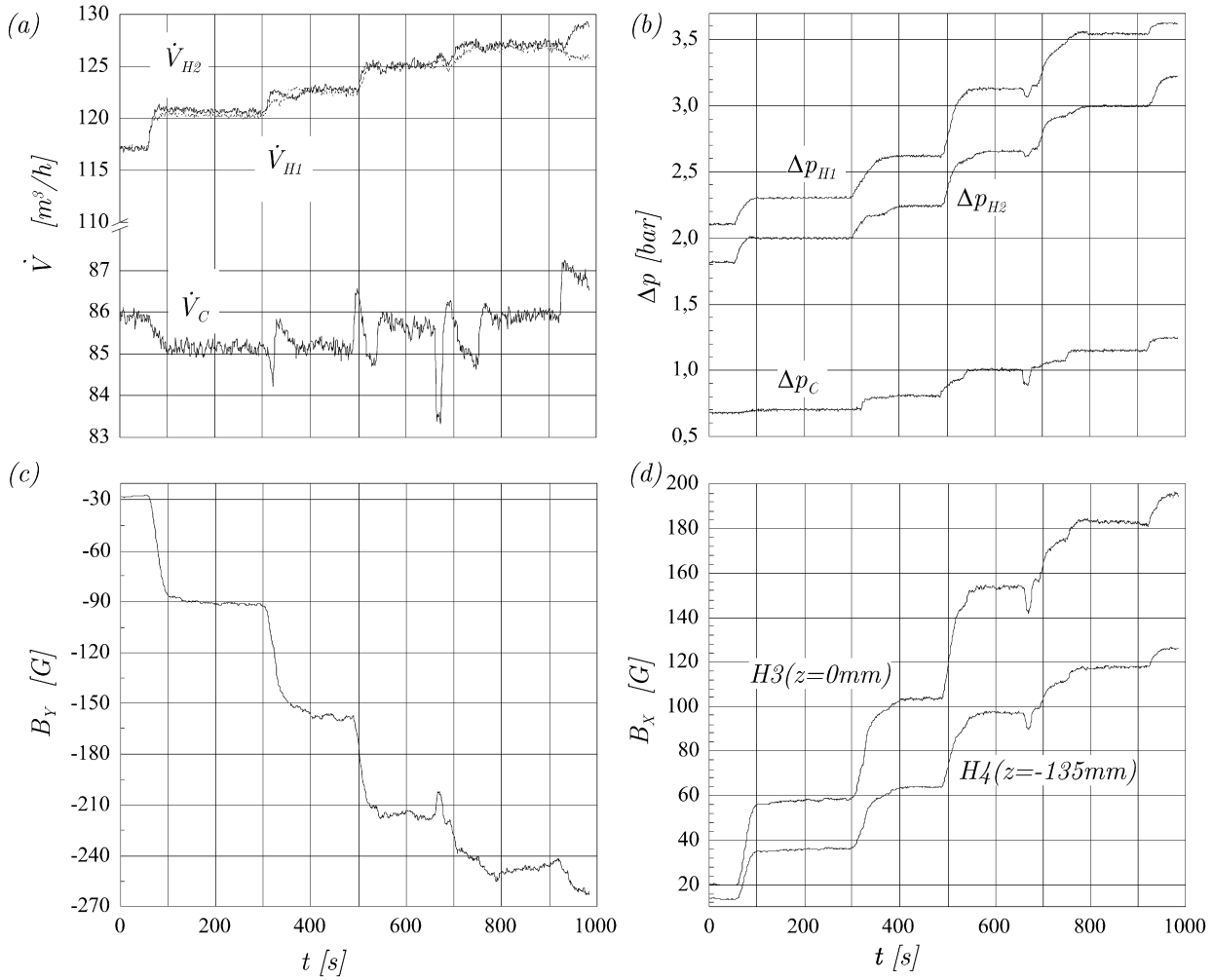


Fig. 2. Time signals for (a) volumetric flow rates, (b) pressure losses, (c), (d) magnetic field components $B_X$, $B_Y$ for stepwise changing flow rates.

by a Hall-probe, as a function of the axial and helical volumetric flow rates. Keeping the axial flow rate constant and raising the helical flow rate stepwise after certain time intervals initiates a magnetic field when a threshold flow rate was exceeded. Each further increase of the flow rate results in another increase of the magnetic field intensity and a following adjustment to a new equilibrium plateau. The critical conditions for the onset of dynamo action can be recognized experimentally by the sudden increase of the measured local energy density of the magnetic field in the module center and, moreover, from an abrupt change of the measured pressure loss in the helical and central conduits of the module for increasing flow rates.

A graphical extrapolation of the curve branches in the sub and super-critical range determines the critical condition. This is demonstrated in Fig. 3.

The results from several test series for constant axial and varying central flow rates are summarized in the dynamo state diagram of Fig. 4. The solid line marks the fitted best estimate boundary for onset of dynamo action according to the pressure loss and the magnetic energy criterion.

### *3.2. Structure of the magnetic field*

The spatial structure of the magnetic field can be inferred from the intensity distribution of its components along the axis of the module. This is shown for a specific volumetric flow rate in Fig. 5.

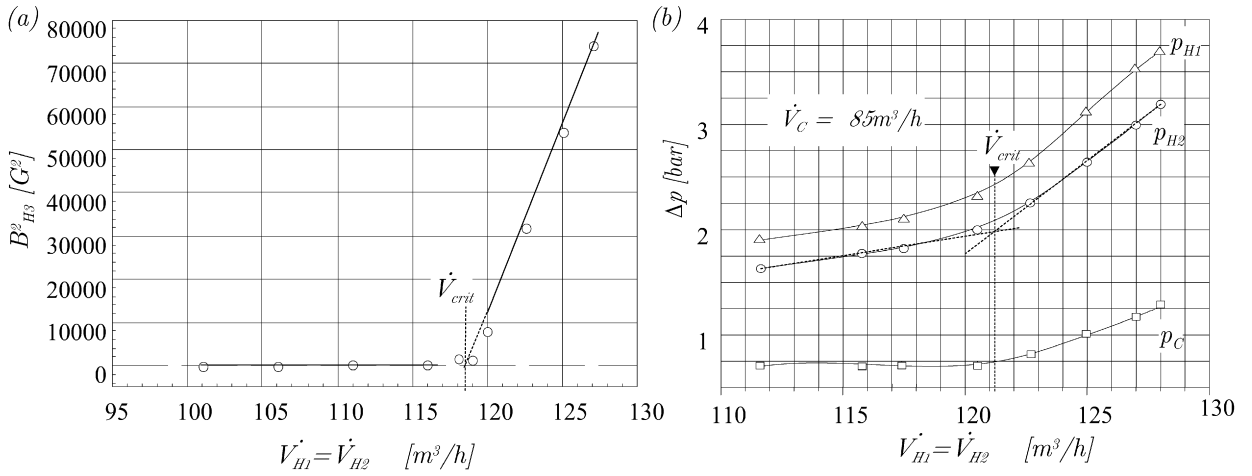


Fig. 3. (a) The square of the magnetic induction $B^2$ in the centre of the module. (b) Pressure losses $\Delta p$ in the helical and central piping systems for steady state operation. Straight lines fit the data points. Their intersections mark the critical condition.

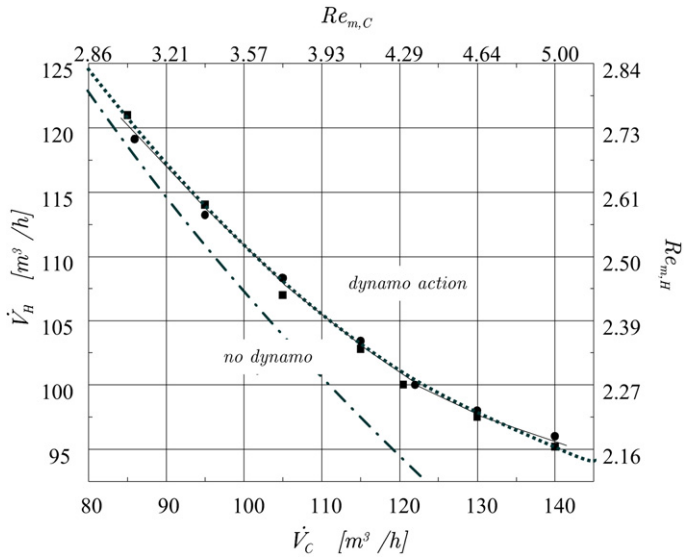


Fig. 4. State diagram for dynamo action in terms of operational volumetric flow rates or related magnetic Reynolds numbers. Experimental data: ● energy criterion; ■ pressure criterion. Solid line shows fit to experimental data. Dotted and dash-dotted lines mark theoretical predictions by Tilgner [19] and Rädler et al. [21].

There is only a very small axial component $B_Z$ of the magnetic field and, as seen in Fig. 5(b), the radial component $B_r = (B_X^2 + B_Y^2)^{1/2}$ is twisted around the axis in a staircase manner from the upper lid of the cylinder at $z = 0.5$ m to the center at $z = 0$ and presumably beyond. As seen in Fig. 5(a) the distribution is not fully symmetric as to be expected for a perfectly symmetric arrangement of the vortex generators. This can technically not be achieved, however, owing to the inlet and outlet connecting piping system as illustrated in Fig. 1(c). A characteristic feature of the magnetic field outside the test module was identified by measuring the normal component of the field with regard to an $(x, z)$-plane realized by a wooden board placed vertically and sideways of the cylinder surface line at a distance 1.67 m from the axis. The measurements were taken with the aid of a movable Gauss meter.

The iso-lines are presented in Fig. 6(a). The iso-line pattern indicates that the magnetic field has dipole character with the main dipole direction perpendicular to the cylinder axis, slightly inclined to the $y$-axis and nearly centered in the middle of the module.

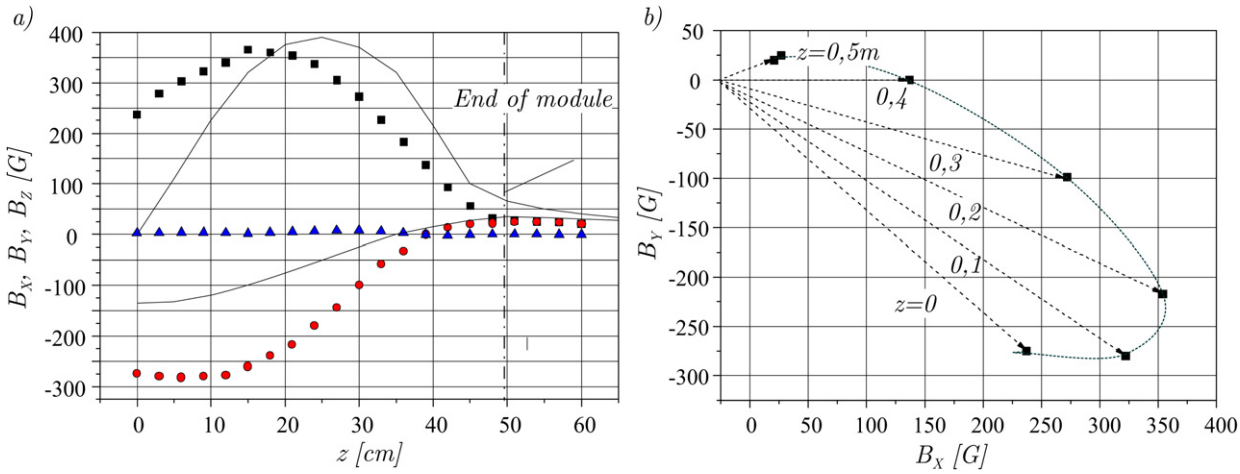


Fig. 5. (a) Measured components of the magnetic induction $B_X$ (■), $B_Y$ (●) and $B_Z$ (▲) along the module axis in the range $0 < z < 0.60$ m for the volumetric flow rates $\dot{V}_C = \dot{V}_H = 111\ \mathrm{m}^3/h$. Solid and dashed lines show calculated values of Tilgner [19], (b) orientation of the magnetic field along the module axis in the range $0 \leqslant z \leqslant 0.5$ m.

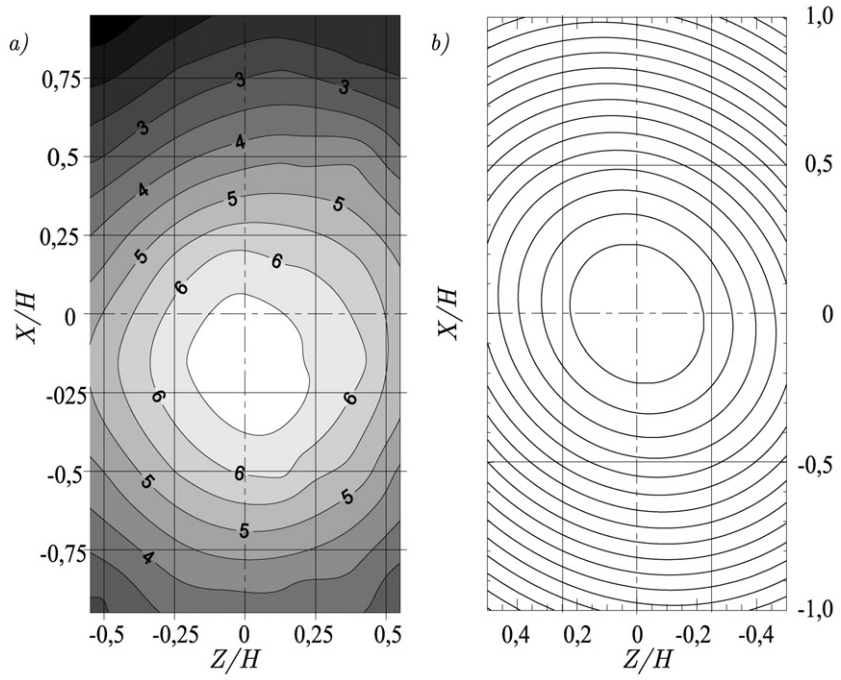


Fig. 6. Demonstration of the global structure of the dynamo magnetic field, (a) measured iso-lines of $B_Y$ in a vertical plane 1.6 m off the centre axis. (b) Calculated iso-lines for corresponding experimental conditions of Tilgner [19].

More subtle features of the dynamo magnetic field were realized by artificially perturbing the initial environmental seed magnetic field or even an already generated weak dynamo field by means an external magnetic field provided by two Helmholtz coils placed sideways of the test module. Starting from the environmental seed field and running in steps through a sequence of fixed supercritical flow rates saturated steady magnetic field states were observed after a short temporal transition. With increasing flow rates the saturated dynamo field intensities grew first weakly, then hefty and finally settled down tending to approach a saturation. This procedure is demonstrated in Fig. 7(a) by the lower branch of a sequence of measured values of the $B_Y$-component. If at some supercritical state an external Helmholtz magnetic field of opposite direction was suddenly turned on, the dynamo magnetic field changed direction

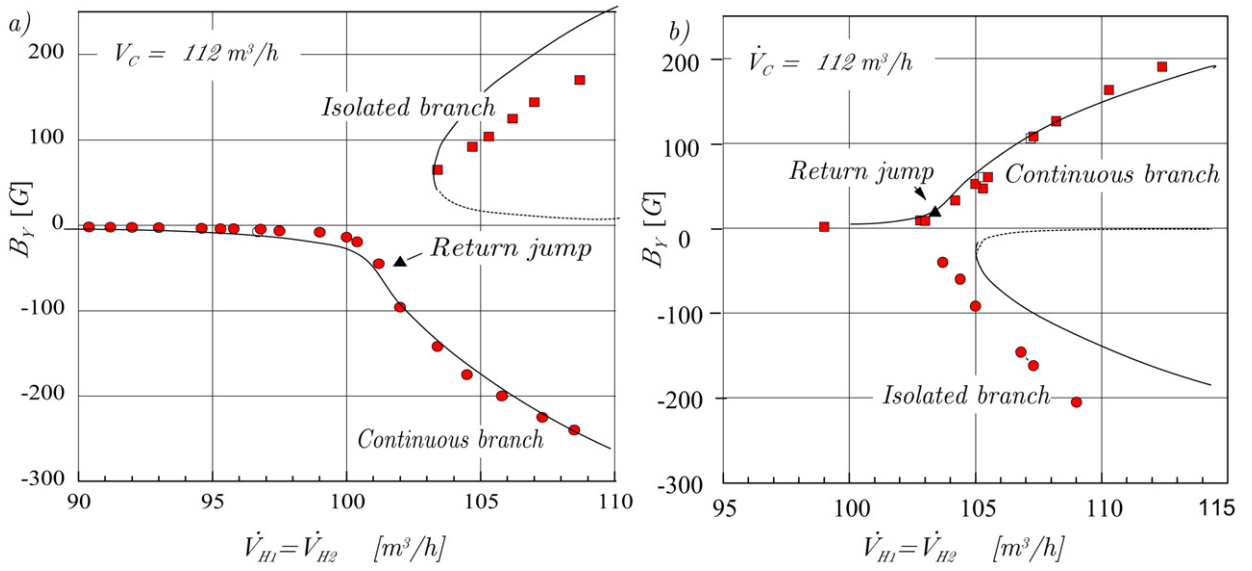


Fig. 7. The bifurcation process of dynamo action represented by the local $B_Y$-component in the centre of the module: ●, ■ stationary states on a continuous and an isolated branch respectively. ▲ marks the return jump from the isolated to the continuous branch. (a) Initial condition: the natural environmental seed magnetic field, parameter range $\dot{V}_C = 112.5\ \mathrm{m}^3/h$, $92 < \dot{V}_{H1,2} < 110\ \mathrm{m}^3/h$. Solid/dashed lines show model calculations by Tilgner and Busse [17], (b) initial condition: a Helmholtz-coil seed field, parameter range $\dot{V}_C = 112.5\ \mathrm{m}^3/h$, $98 < \dot{V}_{H1,2} < 113\ \mathrm{m}^3/h$. Solid/dashed lines give model calculations by Rädler et al. [20].

and maintained this state even after the external field was switched off. A whole sequence of stable dipole states was realized when increasing or decreasing the flow rates. However, when the flow rates were reduced below a certain threshold value the dynamo dipole field switched direction as a transition to the lower continuous branch of stable dynamo states occurred. Fig. 7(a) demonstrates typically the imperfect bifurcation mechanism from a purely hydrodynamic channel flow to a state of dynamo action. It also underlines the non-symmetry of the test module. Here, the essential observation is the existence of two nearly equivalent dipole states in a certain range of volumetric flow rates. Changing the initial conditions and starting from a strong enough seed field provided by the Helmholtz coils a mirror symmetric bifurcation process for dynamo action was observed. This is seen in Fig. 7(b) and underscores the dual dipole character of the Roberts–Busse dynamo (Müller et al. [28]).

### *3.3. Back-reaction and Joule dissipation*

Key issues of hydrodynamically forced kinematic dynamos are the way the magnetic field feeds back on the channel flow by Joule dissipation losses and, furthermore, on the velocity redistribution in the channels of the vortex generators. Such effects finally limit the growth rate of the dynamo magnetic field energy. The Joule dissipation, which has to be considered as the major source in the saturation process of the dynamo magnetic field, can be evaluated from the measured pressure losses and the related volumetric flow rates in the flow channels. As a result the total Joule dissipation for the continuous branch of the test series of Fig. 7(a) is depicted in Fig. 8(a) as function of the flow rates. It increases linearly in the super-critical range as does the local magnetic energy density (see also Fig. 2(a)) and thus indicates its $|B^2|$-proportional quenching effect on the dynamo action. Its portion of the total dissipation, that is the viscous plus Joule dissipation, achieves nearly 50% for the highest realized flow rates.

The feed back on the velocity was investigated by placing a permanent magnet potential probe in the centre of one of the axial channels next to the center of the module. From the recorded voltage signal of the probe the local velocity in the center of the channel was determined (see Müller et al. [23]). The measured relative local velocity, presented in Fig. 8(b) as a function of the helical flow rate in the sub- and super-critical range, shows that the normalized velocity remains at the same value in the sub-critical range $\dot{V}_H < 106\ \mathrm{m}^3/h$. Beyond this threshold the velocity decreases rapidly and then approaches another lower saturation value. A reasonable explanation for this observation is that the Lorenz forces induced by the dipole magnetic field flatten the turbulent velocity profile in the axial channel towards

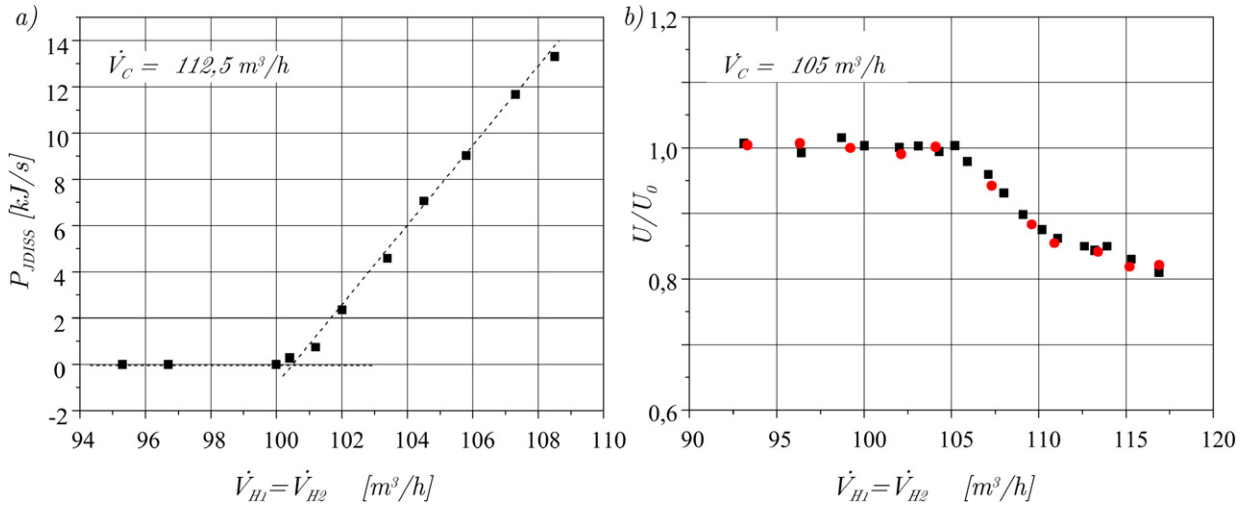


Fig. 8. (a) Joule dissipation for increasing helical flow rates and for a constant central flow rate $\dot{V}_C = 112.5\ \mathrm{m}^3/h$ corresponding to Fig. 7(a). (b) Measured relative reduction of the axial velocity in the centre of a vortex generator located next to the module axis for increasing helical flow rates and a central flow rate $\dot{V}_C = 105\ \mathrm{m}^3/h$.

a piston like Hartmann velocity profile. The decrease of about 17% is in fair agreement with a relationship for fully developed turbulent pipe flow and the associated mean flow given as $\bar{u} = 0.84 u_{\max}$ for a Reynolds number $Re = 10^6$ with $u_{\max}$ the maximum velocity in the pipe centre and the mean velocity $\bar{u}$ (see e.g. Schlichting [24]).

### *3.4. Temporal fluctuations of saturated dynamo states*

The saturated dynamo states are steady in the time average, but fluctuate about a mean value of the magnetic field. Typical segments of a time series records for $B_Y$ and $B_Z$ at volumetric flow rates $\dot{V}_C = \dot{V}_{H1} = \dot{V}_{H2} = 115\ \mathrm{m}^3/h$ are shown in Fig. 9. The quality of the fluctuations may be judged by the probability density function (PDF), the standard deviation (RMS), the skewness and flatness. An analysis has shown (Müller et al. [29]) that characteristic features of the signals of Fig. 9 are a quasi-Gaussian PDF with a vanishing skewness, a constant flatness of 2.5 and a constant RMS value $B'_Y = 0.58G$. The latter has to be compared with the mean value $B_Y = 260G$ which gives a small relative fluctuation level of about 0.2%. When evaluating RMS values at other equal but lower flow rates it has been observed, however, that this level is larger for the $z$-component $B_Z$ and for all components near the onset of self-excitation. Fig. 10 shows the standard deviations of magnetic field components together with their corresponding mean values for an up-scan sequence of dynamo equilibrium states. The graphs indicate clearly that for higher flow rates the RMS values achieve a saturation level faster than the corresponding mean components of the field. This feature can be quantified by normalizing the RMS value by the corresponding mean values. Evaluated normalized RMS values have shown a decrease with increasing flow rates. From this observation it may be inferred that the increasing intensity of the mean magnetic field limits the growth rate of its turbulent fluctuations and even dampens them. This observation may be interpreted in terms of a feed-back chain between the magnetic field and the sodium velocity. On the one hand the mean magnetic field dampens the velocity fluctuations on the other hand the remaining velocity fluctuations still induce small temporal variations of the magnetic field. This idea gets support from spatial cross-correlation measurements between time signals of Hall- and PM-probes. Even at strong dynamo action a small but significant correlation was observed for small probe distances of the order of channel diameters (Müller et al. [23]).

## 4. Discussions

Apart from its demonstrative character the Karlsruhe Dynamo Experiment has provided observations and data that may be used to test and validate theoretical models for homogeneous dynamo action. This has been done by Tilgner and Busse and Rädler and his collaborators. Tilgner [17,18] used a spectral method to solve the induction equation for a suitably modeled velocity distribution in circular cylindrical containers of aspect ratios $R/H = 1$ and $R/H = 1.2$ embedded in a spherical volume tangent to their circular rims. He calculated the marginal state for the onset of dynamo

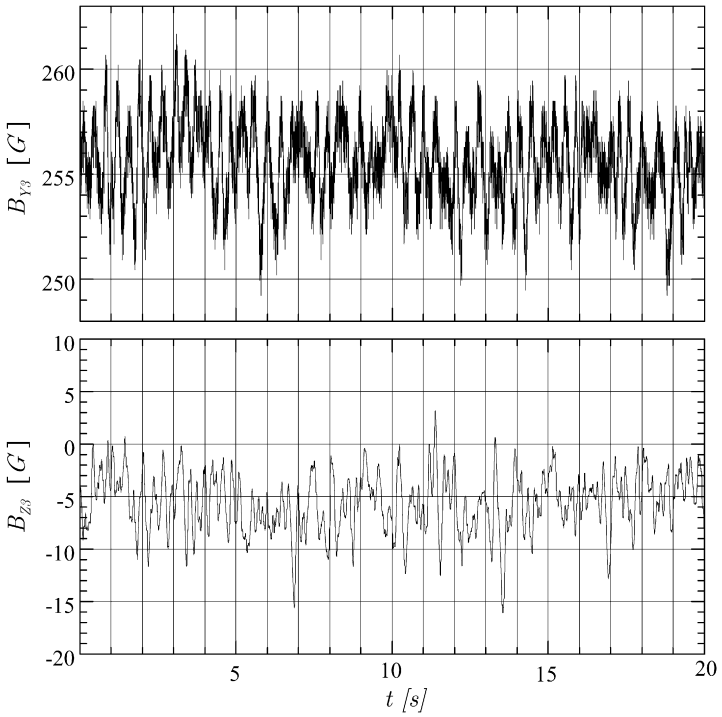


Fig. 9. Typical time signals of the components $B_Y$ and $B_Z$ of the magnetic field recorded by the Hall probes in the centre of the test module at constant flow rates $\dot{V}_C = \dot{V}_H = 115\ \mathrm{m}^3/h$.

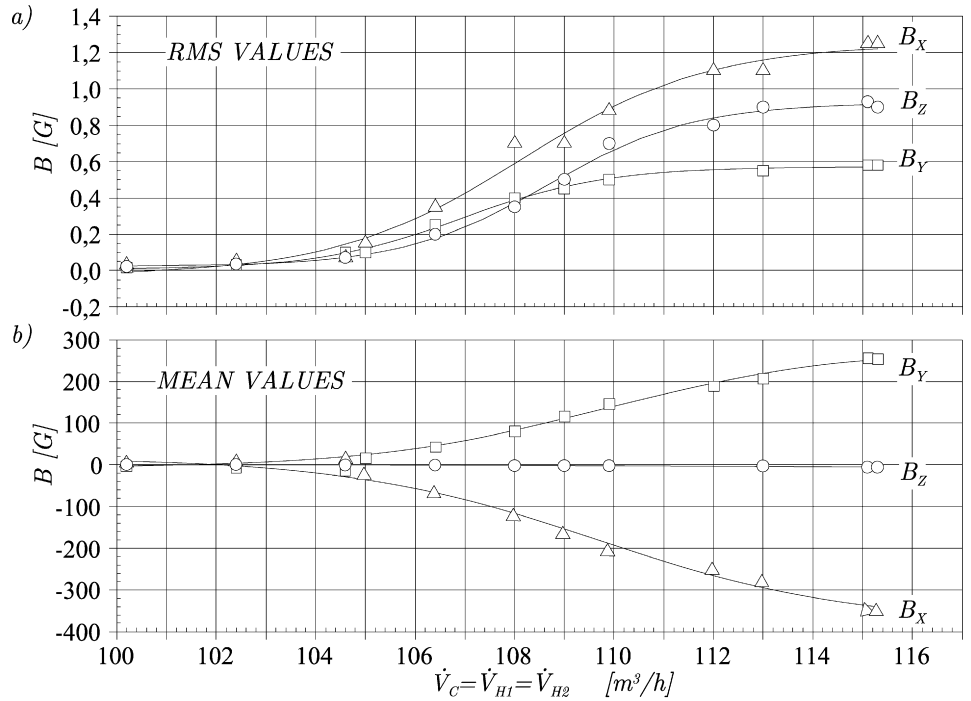


Fig. 10. (a) The standard deviation (RMS) of the time signals of the magnetic field components $B_X$, $B_Y$, $B_Z$ as a function of the flow rates; (b) Their associated mean values.

action as a function of the relevant axial and helical flow rates and tested the sensitivity of this marginal boundary against slight modifications of velocity distributions, moderate changes of the magnetic diffusivity of the working fluid with regard to hydraulic turbulences and slight variations of the aspect ratios accounting for deviations between the geometries of the actual technical design and the idealized model container. Within the range of realized flow rates in the test runs there is generally a good agreement between the calculated and experimental findings. A nearly complete agreement is achieved for the parameter set $R/H = 1.2$, $\lambda = 0.1\ \mathrm{m/s^2}$ and a velocity distribution of the helical flow modeled according to solid body rotation. This is documented in Fig. 4 by the dotted line. Thus, the onset of dynamo action is well predicted.

Furthermore, the calculations produce a magnetic field of dipolar character oriented perpendicular to and twisted around the cylinder axis by an angle. Its axial component vanishes on the cylinder axis and it is degenerate with regard to its general radial orientation. As outlined above the observed magnetic field has also dipolar orientation perpendicular to the cylinder but its axis was always fixed independently of the different starting and operational conditions if only the helical flow rates were equal. This fixing was caused by asymmetries in the technical device, in particular those given by the inlet and outlet piping system of the module. Moreover, the axial distribution of the observed magnetic field intensity is phase shifted compared to the calculated field components. This is seen in Fig. 5(a) which shows measured and calculated field components on the cylinder axis. Nevertheless the observed dipole field is well simulated numerically as is seen in Fig. 6(b) which shows iso-lines of the magnetic potential in an $(x, z)$-plane at $y = 1.67$ m corresponding to the measured iso-line graph of Fig. 6(a). Except for minor differences in the location of the centre of the set of closed iso-lines the overall character of the dipole field in this particular plane in well simulated, taking into account that even the strongest asymmetry of the technical dynamo device, the inlet and outlet piping system, was not accounted for in the model geometry of the computations (see also Tilgner [18]).

Rädler and collaborators [21,22] employed mean field methods (Krause and Rädler [30]) to simulate the experimental observations. The temporal and/or spatial averaging of evolution equations, here the induction equation, leads to closure problems for averaged products of fluctuation terms. Their representation in terms of the averaged mean variables, here the mean magnetic field components, is the key issue of this model approach and requires in general multi-parameter expansions of the correlations depending on the required accuracy of the simulation. The crucial quantity for dynamo excitation to be modeled in this way is the driving mean electromotive force. As outlined in detail by Rädler et al. [22] the adequate description of the marginal conditions for dynamo action in terms of critical volumetric flow rates requires the evaluation of six expansion coefficients. Three parameters ($\alpha$-effects) then account first of all for a most likely velocity distribution in the experimental spin generators including end effects at the confining boundaries of the cylindrical model geometry. The enhancement of the electrical conductivity by flow turbulence enters the model approach by three more parameters ($\beta$-effects). With these parameters taken into account and by means of the induction equation for the mean field the authors derive a best estimate lower bound for the onset of dynamo action as displayed in Fig. 4 by the dash-dotted line. The best estimate curve still underestimates the measured data. Moreover, it shows a less steep gradient compared to the experimental and Tilgner's numerical curve. Rädler and collaborators [22] explain the latter effect by obvious limitations of a second order approximation for the electromotive force with regard to the relatively poor separation of scales realized in the experimental set up. It shall, however, be emphasized that the topological structure of the magnetic field and its dipole character is equally well predicted by the mean field theory and by Tilgner's direct spectral method.

Dynamo action in the supercritical range of flow rates is governed by the feedback of the induced magnetic field on the velocity and pressure field in the test volume through Lorentz forces. Thus, a force balance has to be performed, together with a solution of the induction equation in order to capture the non-linear evolution and saturation effects, observed in the experiments, by analytical and numerical models. Using spectral methods, Tilgner [18] achieved this by solving simultaneously the Navier–Stokes-equations (N.S.) and the induction equation in the relevant flow domain with the assumption that a basic quasi-periodic flow pattern is enforced to the system by an adequate forcing term in the N.S.-equations. This enabled him to model semi-quantitatively the observed saturated mean dynamo states of both branches in Fig. 7(a) as well as transitions between states on the two branches, i.e. dipole inversions, induced by seed field perturbations or by falling below the critical flow rates for states on the isolated branch. The continuous lines in Fig. 7(a) show the bifurcation diagram in comparison with the experimental data. Considering the complexity of the technical design and the simplifying assumptions in the model, the experimental data set is well approximated by the model curves.

Rädler et al. [22] utilize the mean field theory to analyze the super-critical saturation mechanism of the observed dynamo magnetic field. By introducing an $\alpha$-quenching which represents the reduction of the $\alpha$-effect with increasing magnetic field strength they obtain a fifth order algebraic equation for the intensity of the mean induced magnetic field. Taking into account the specific parameters of the technical device and the particular test conditions they derive a diagram for the steady, saturated supercritical dynamo states shown as the continuous lines in Fig. 7(b) that, on the whole, compares well with the experimental findings.

The numerical simulation of the feed-back of the mean dynamo magnetic field on the local velocity as demonstrated by the experimental data of Fig. 8(b) and the interaction of velocity fluctuations and the magnetic field is presently beyond the available computing capacities for geometries as complex as the Karlsruhe test module. Moreover, as the flow in the channels is highly turbulent, there is the need to either solve the hydromagnetic dynamo equations by direct numerical methods or to utilize sophisticated procedures for modeling simultaneously the anisotropic turbulence of the velocity and the magnetic field which either exceed the current computing capabilities for geometries as complex as the Karlsruhe test module or are not yet available in the literature. However, it shall be stressed that for the highly constrained flow in the Karlsruhe dynamo module the assumption of laminar velocity distribution in model calculations catches all the essentials of dynamo action and that small scale flow turbulence may add only minor corrections (see Tilgner [31]).

Nevertheless, clarification of the fundamental question, how fluid flow turbulence acts on a dynamo magnetic field and vice versa, is certainly a challenge for the physical and numerical modeling of turbulence and for the new generation of dynamo experiments that are based on impeller driven highly turbulent vortex flows in cylindrical or spherical containers. In particular, the experiments are expected to elucidate this issue. This special CRAS issue is dedicated to reporting the progress of some of them (for details of other concerning experimental programs see also e.g. the special issue of Magnetohydrodynamics [32].

## Acknowledgements

The authors thank Cambridge University Press for permitting reproduction of Figs. 1, 2, 3, 5, 7, 9 and 10 from their publication [29] in the Journal of Fluid Mechanics.

## References

[1] J. Larmor, Rep. Brit. Assos. Adv. Sci. (1919) 159–160.
[2] P.H. Roberts, in: R.E. Proctor, A.D. Gilbert (Eds.), Lectures on Solar and Planetary Dynamos, Cambridge Univ. Press, 1994, pp. 1–58.
[3] P.H. Roberts, G.A. Glatzmaier, Rev. Mod. Phys. 72 (2000) 1081–1123.
[4] F.H. Busse, Phys. Fluids 14 (2002) 1301–1314.
[5] G. Glatzmaier, Ann. Rev. Earth Planet. Sci. 30 (2002) 337–357.
[6] F.H. Busse, C.R. Carrigan, J. Fluid Mech. 62 (1974) 579–592.
[7] C.R. Carrigan, F.H. Busse, J. Fluid Mech. 126 (1983) 287–305.
[8] A. Gailitis, Magnétohydrodynamiques 3 (1967) 23–29.
[9] G.O. Roberts, Phil. Trans. R. Soc. Lond. A 266 (1972) 535–558.
[10] F.H. Busse, Geophys. J. Astron. Soc. 42 (1975) 437–459.
[11] F.H. Busse, Annu. Rev. Fluid Mech. 10 (1978) 435–462.
[12] U. Christensen, P. Olson, A. Glatzmaier, Geophys. J. Int. 138 (1999) 393–409.
[13] J. Aubert, D. Brito, H. Nataf, P. Cardin, J. Masson, Phys. Earth. Planet. Int. 128 (2001) 51–74.
[14] F.H. Busse, Internal Report Kernforschungszentrum Karlsruhe, Sept. 1979.
[15] F.H. Busse, in: R. Friederich, A. Wunderlin (Eds.), Dynamical Structures in Complex Systems, Springer, 1992, pp. 359–384.
[16] A. Tilgner, Acta Astron. Geophys. Univ. Comenianae 19 (1997) 51–62.
[17] A. Tilgner, Phys. Lett. A 226 (1997) 75–79.
[18] A. Tilgner, Phys. Fluids 14 (2002) 4092–4094.
[19] A. Tilgner, F.H. Busse, Magnetohydrodynamics 38 (2002) 35–40.
[20] K.H. Rädler, A. Apel, E. Apstein, M. Reinhard, Sci. Rep. Astrophys. Inst. Potsdam (1996).
[21] K.H. Rädler, E. Apstein, M. Reinhard, M. Schüler, Stud. Geophys. Geod. 42 (1998) 224.
[22] K.-H. Rädler, E. Rheinhard, E. Apstein, H. Fuchs, Magneto-Hydro-Dynamics 38 (2002) 41–71 and 73–94.
[23] U. Müller, R. Stieglitz, S. Horanyi, J. Fluid Mech. 552 (2006) 419–440.
[24] H. Schlichting, Grenzschicht-Theorie, in: G. Braun, Karlsruhe, 1958, p. 467.
[25] R. Stieglitz, U. Müller, Wiss. Bericht FZKA 5716, 1996.
[26] U. Müller, R. Stieglitz, Naturwissenschaften 87 (2000) 381–390.

[27] R. Stieglitz, U. Müller, Phys. Fluids 13 (2001) 561–564.
[28] U. Müller, R. Stieglitz, S. Horanyi, Wiss. Ber. Forschungszentrum, FZKA 6756, 2002.
[29] U. Müller, R. Stieglitz, S. Horanyi, J. Fluid Mech. 498 (2004) 31–71.
[30] K. Krause, K.H. Rädler, Mean-Field Magnetohydrodynamics and Dynamo Theory, Pergamon Press, Oxford, 1980.
[31] A. Tilgner, New J. Phys. 9 (2007), 1367-2639/07/010000.
[32] A. Cebers, K.H. Rädler, Magnetohydrodynamics 38 (2002) 1–2.